

Differentially Disrupted Functional Connectivity in Posteromedial Cortical Subregions in Alzheimer's Disease

Mingrui Xia^{a,b}, Zhiqun Wang^c, Zhengjia Dai^{a,b}, Xia Liang^{a,b}, Haiqing Song^d, Ni Shu^{a,b}, Kuncheng Li^{c,*} and Yong He^{a,b,*}

^aState Key Laboratory of Cognitive Neuroscience and Learning & IDG/McGovern Institute for Brain Research, Beijing Normal University, Beijing, China

^bCenter for Collaboration and Innovation in Brain and Learning Sciences, Beijing Normal University, Beijing, China

^cDepartment of Radiology, Xuanwu Hospital of Capital Medical University, Beijing, China

^dDepartment of Neurology, Xuanwu Hospital of Capital Medical University, Beijing, China

Handling Associate Editor: Lies Clerx

Accepted 25 September 2013

Abstract. Neuroimaging studies have demonstrated that patients with Alzheimer's disease (AD) have remarkable focal grey matter loss and hypometabolism in the posteromedial cortex (PMC), which is composed of the precuneus and posterior cingulate cortex, suggesting an important association of the PMC with AD pathophysiology. Studies have also shown that the PMC is a structurally and functionally heterogeneous structure containing various subregions with distinct connectivity profiles. However, whether these PMC subregions show differentially disrupted connectivity patterns in AD remains largely unknown. Here, we addressed this issue by collecting resting-state functional MRI data from 32 AD patients and 38 healthy controls. We automatically identified the PMC subregions using a graph-based module detection algorithm and then mapped the whole-brain functional connectivity pattern of each subregion. The functional connectivity analysis was followed by a hierarchical clustering analysis to classify each subregion. Three distinct spatial connectivity patterns were observed across the PMC subregions: the anterior dorsal zone was functionally connected with the sensorimotor cortex; the posterior dorsal zone was functionally connected with the frontoparietal cortex; and the central and ventral zones were functionally connected with the default-mode regions. Group comparison analysis revealed that all three functional systems were significantly disrupted in the AD patients compared to the controls and these disruptions were positively correlated with the patients' cognitive performance. Collectively, we showed that the subregions of the PMC exhibit differentially disrupted neuronal circuitry in AD patients, which provides new insight into the functional neuroanatomy of the human PMC and the alterations that may be relevant to disease.

Keywords: Alzheimer's disease, connectome, dementia, functional magnetic resonance imaging, network, parietal lobe

INTRODUCTION

Alzheimer's disease (AD) is a progressive neurodegenerative disease characterized by a decline in memory and cognitive functions. Many studies have demonstrated that this decline is associated with regional grey matter (GM) reductions and functional abnormalities in various brain regions [1, 2]. Recent

*Correspondence to: Yong He, PhD, State Key Laboratory of Cognitive Neuroscience and Learning & IDG/McGovern Institute for Brain Research, Center for Collaboration and Innovation in Brain and Learning Sciences, Beijing Normal University, Beijing 100875, China. Tel.: +8610 5880 2036; E-mail: yong.he@bnu.edu.cn or Kuncheng Li, MD, Department of Radiology, Xuanwu Hospital of Capital Medical University, Beijing 100053, China. E-mail: likuncheng@xwh.ccmu.edu.cn.

studies investigating inter-regional relationships suggest that AD is a syndrome of disconnection in brain networks [3, 4]. Using resting-state functional magnetic resonance imaging (R-fMRI), a promising imaging technique that measures the brain's spontaneous activity, studies have revealed AD-related disruptions of resting-state functional connectivity (RSFC) in the hippocampus [5], medial prefrontal cortex (MPFC) [6], and particularly in the posteromedial cortex (PMC) [7–9].

The PMC in humans, which is composed of the pre-cuneus (PCu) and posterior cingulate cortex (PCC), has long been known as a major association area that serves a variety of behavioral functions [10] and exhibits high glucose metabolism [11] and oxygen consumption [12]. Studies have suggested that PMC is involved in a wide spectrum of integrated functions, including motor execution [13], memory retrieval [14, 15], and self-consciousness [16]. Recently, the PMC has been considered a core component of the default-mode network (DMN) [12, 17] and has also been identified as a critical hub in human whole-brain structural [18–20] and functional [21, 22] networks. All of these findings imply that the PMC plays an important role in the integration of brain functions.

Anatomical tracing studies in monkeys have shown that the PMC is a heterogeneous structure consisting of several specific subregions, with each subregion exhibiting distinct structural connectivity patterns [23–25]. Using diffusion magnetic resonance imaging (dMRI) data from humans, Zhang et al. [26] subdivided the PMC into several subregions that were distinctly and structurally connected with sensorimotor, frontal-parietal, DMN, and visual regions. Using human R-fMRI data, several studies have suggested that PMC subregions have different RSFC patterns [27–29]. Intriguingly, despite the different imaging modalities, species, and computational methods used in these studies, the results of the PMC parcellation were largely comparable. Although numerous neuroimaging studies have demonstrated AD-related

alterations of PMC connectivity, it remains largely unknown whether the connectivity patterns of PMC subregions are differentially disrupted in AD.

Here, we employed R-fMRI to investigate the RSFC patterns of the PMC subregions in AD patients and healthy controls. We identified PMC subregions using a graph-based module detection method and then explored the RSFC pattern of each subregion. Furthermore, we examined between-group differences in the RSFC of each PMC subregion and any behavioral correlates.

MATERIALS AND METHODS

Subjects

Thirty-four patients with AD and forty-one healthy controls (HCs) were recruited after giving written informed consent. The study was approved by the Medical Research Ethics Committee of Xuanwu Hospital. Data from five subjects (2 AD patients and 3 HCs) were excluded due to the failure of imaging processing (see image pre-processing). Clinical and demographic data for the remaining 70 participants (32 AD patients and 38 HCs) are shown in Table 1. A subset of the dataset (16 AD patients and 22 HCs) was previously used to study the impairment of regional brain activity in AD [30]. AD patients were recruited from a population of individuals who had consulted a memory clinic at Xuanwu Hospital for memory complaints and underwent a complete physical and neurological examination, including standard laboratory tests. The diagnosis of AD fulfilled the Diagnostic and Statistical Manual of Mental Disorders 4th Edition criteria for dementia and the National Institute of Neurological and Communicative Disorders and Stroke/Alzheimer Disease and Related Disorders Association (NINCDS-ADRDA) criteria for possible or probable AD [31, 32]. The patients were assessed with the Clinical Dementia Rating (CDR) [33] and scored as being in the early stages of AD (14 patients with CDR = 0.5 and

Table 1
Demographics and clinical characteristics

	AD (<i>n</i> = 32)	HC (<i>n</i> = 38)	<i>p</i> value
Age (years)	52–86 (71.25 ± 8.63)	50–86 (68.39 ± 7.78)	0.15 ^a
Gender (male/female)	14/18	13/25	0.41 ^b
CDR	0.5–1 (0.78 ± 0.25)	0	<0.001 ^a
MMSE	10–25 (18.56 ± 3.99)	28–30 (28.63 ± 0.67)	<0.001 ^a

Data are presented as the range of minimum – maximum (mean ± SD). AD, Alzheimer's disease; HC, healthy control; CDR, Clinical Dementia Rating Scale; MMSE, Mini-Mental State Examination. ^aThe *p* value was obtained by two-sample two-tailed *t* test. ^bThe *p* value was obtained by two-tailed Pearson chi-square test.

18 patients with CDR = 1). The inclusion criteria for HCs were as follows: (1) no neurological or psychiatric disorders such as stroke, depression or epilepsy; (2) no neurological deficiencies such as visual or hearing loss; (3) no abnormal findings such as infarction or focal lesion in conventional brain MR imaging; (4) no cognitive complaints; (5) Mini-Mental State Examination (MMSE) score of 28 or higher; and (6) a CDR score of 0.

Data acquisition

MRI data acquisition was performed on a SIEMENS Trio 3-Tesla scanner (Siemens, Erlangen, Germany). Foam padding and headphones were used to limit head motion and reduce scanner noise. Functional images were collected axially using an echo-planar imaging (EPI) sequence with the following parameters: repetition time (TR) = 2000 ms, echo time (TE) = 40 ms, flip angle (FA) = 90°, field of view (FOV) = 24 × 24 cm², resolution = 64 × 64 matrix, slices = 28, thickness = 4 mm, voxel size = 3.75 × 3.75 × 4 mm³, gap = 1 mm, and bandwidth = 2232 Hz/pixel. The subjects were required to remain still, keep their eyes closed, and not think of anything in particular during the 478 s resting scan. According to a simple questionnaire after the scan, none of the subjects had fallen asleep. High-resolution structural images were collected using a 3D magnetization-prepared rapid gradient echo (MPRAGE) T1-weighted sequence with the following parameters: TR = 1900 ms, TE = 2.2 ms, inversion time (TI) = 900 ms, FA = 9°, resolution = 256 × 256 matrix, slices = 176, thickness = 1 mm, and voxel size = 1 × 1 × 1 mm³.

Data pre-processing

Data preprocessing was carried out using the Statistical Parametric Mapping (SPM, <http://www.fil.ion.ucl.ac.uk/spm>) and Data Processing Assistant for Resting-State fMRI (DPASF, <http://www.restfmri.net/forum/DPARSF>) [34] toolkits. Image preprocessing consisted of the following steps: (1) discard the first ten volumes of each subject for scanner stabilization and to allow participants to adapt to the scanning; (2) correct slice acquisition dependent time shifts using Fourier interpolation; (3) correct head motion using a least-squares approach and six-parameter linear transformation [35]; (4) co-register individual T1-weighted structural images to the mean realigned functional images using linear transformation; (5) segment the coregistered structural images and nonlinearly nor-

malize to the custom template (see below for custom template generation) using a unified segmentation algorithm [36]; (6) spatially normalize the motion-corrected functional volumes to the custom template and resample to 3 mm isotropic voxels using the nonlinear normalization parameters estimated by step (5); (7) spatially smooth the functional images with a 4 mm full width at half maximum (FWHM) Gaussian kernel; (8) temporal band-pass filter (0.01–0.1 Hz) to reduce the effect of low-frequency drift and high-frequency physiological noise; and (9) regress out several nuisance signals including six head motion parameters, global signal, white matter (WM) signal, and cerebrospinal fluid (CSF) signal [17]. Notably, we generated the custom template for data pre-processing by averaging the normalized structural images across all subjects in MNI space. We obtained the corresponding probability maps of GM, WM, and CSF simultaneously by averaging the segmented structural images across all subjects. The custom template-based registration procedure reduces inaccuracy in the spatial normalization of the functional volumes caused by GM atrophy in our population. During image pre-processing, no subject was excluded based on the 3 mm and 3° head motion criterion, while five subjects (2 AD and 3 HCs) were excluded due to the failure of image normalization.

Automated functional subdivision in PMC

To automatically parcellate the PMC into different subregions, we applied a module detection algorithm based on graph theory. In the brain, different modules usually correspond to groups of anatomically or functionally associated components that perform specific biological functions [37, 38]. Thus, it would be reasonable to consider these functional modules to be different PMC subregions. First, a PMC mask was defined within the custom space based on the PCu and PCC regions (Fig. 1A) of the automated anatomical labeling (AAL) atlas bilaterally [39]. The AAL atlas was transformed from MNI space to the custom space using the inverse transformation matrix estimated during unified segmentation. The PCu and PCC labels (number of voxels, $n = 1,967$) with GM probability (Fig. 1B) greater than 20% were included in the PMC mask (Fig. 1C). Second, for each subject, we extracted the time course of each voxel (Fig. 1D) within the PMC mask and computed the Pearson's correlation coefficient of every pair of time courses. The resulting correlation matrix (1,967 × 1,967) was then converted to z values using Fisher's r-to-z transform.

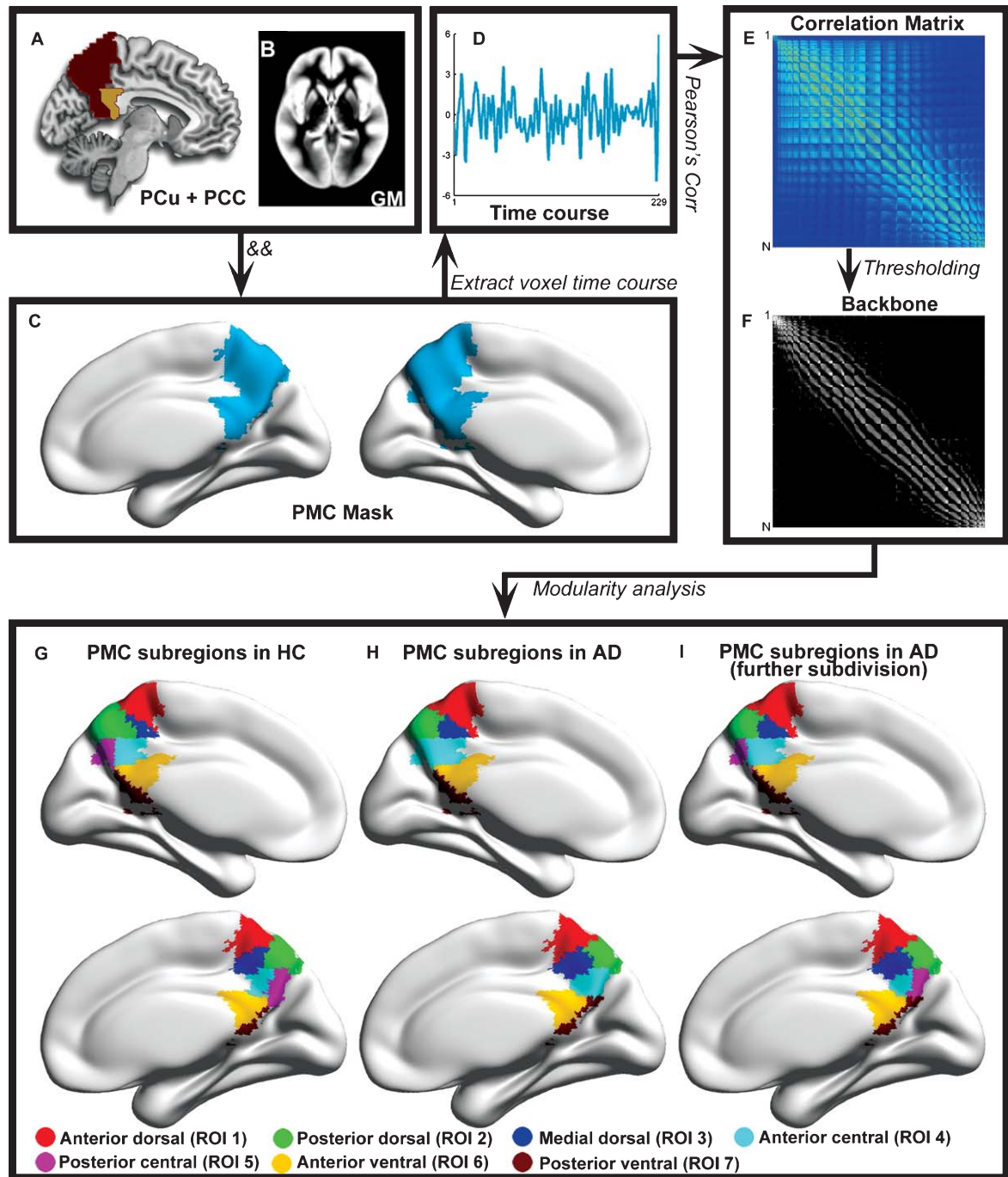


Fig. 1. Automated detection of PMC subregions. A) Voxels labeled PCu or PCC in the AAL atlas with B) a GM probability greater than 0.2 were selected to generate C) the PMC mask. D) The time course of each voxel within the PMC mask was extracted to compute E) the $N \times N$ Pearson's correlation matrix (voxel number, $n = 1967$). F) The backbones of the group-averaged correlation matrices were extracted using a nonparametric method of locally adaptive network sparsification. A modularity analysis algorithm was applied to each backbone matrix to identify PMC subregions. G) Seven PMC subregions were detected in the HC group. H) Six PMC subregions were detected in the AD group. I) Additional subregion detection in the medial posteromedial cortex (colored cyan in H) in AD patients divided this area into two subregions similar to those identified in the HC. G, I) The subdivisions identified in the AD and HC groups were very similar, with a normalized mutual information of 0.86. PMC, posteromedial cortex; PCu, precuneus; PCC, posterior cingulate cortex; GM, grey matter; HC, healthy control; AD, Alzheimer's disease; ROI, region of interest.

Third, group mean z value matrices were obtained by averaging the z value matrices across each cohort (Fig. 1E). The backbone of each group matrix (Fig. 1F) was then extracted using a nonparametric method of locally adaptive network sparsification [40]. Finally, the module detection algorithm [41] was applied to each backbone matrix to identify functional modules (i.e., PMC subregions) in which the temporal correlations were denser within than between them. To further explore whether the subdivision of the PMC was similar between the AD and HC groups, we measured their normalized mutual information (NMI), which quantifies the similarity between the two sets of assignments. Briefly, for a given PMC subregion we first used an index to label all voxels within the subregion. Notably, the subregion labels need to have a spatial correspondence between the two groups. Then, the NMI was calculated as the number of all voxels assigned with the same indices between the two groups divided by the total number of voxels in the PMC mask (i.e., $n = 1967$). The NMI ranges from 0 to 1, where 0 indicates completely different subdivisions and 1 indicates the identification of identical functional subdivisions in each of the two groups. The flowchart of PMC parcellation can be found in Fig. 1. The analyses described in subsequent sections were conducted using the parcellation results of the HC group (Fig. 1G) to obtain the normal parcellation pattern of PMC subregions.

Regional amplitude fluctuations in PMC subregions

We computed the regional amplitude of low-frequency fluctuations (ALFF) in each PMC subregion [42]. Briefly, for a given voxel in the PMC mask, the time course was first extracted and then converted to the frequency domain using a fast Fourier transform. The square root of the power spectrum was computed and averaged across the 0.01–0.1 Hz frequency interval. This averaged square root was taken as the ALFF of the given voxel. To reduce the global effects of variability across participants, the ALFF of each voxel was divided by the global mean ALFF for each subject, as performed in many positron emission tomography (PET) studies [42]. Recently, several R-fMRI studies have shown a high ALFF in the PMC [30, 42, 43] and that the pattern is test-retest reliable across time [44]. In this study, we first computed the ALFF values within the PMC mask in a voxel-wise way using the Resting-state fMRI data analysis toolkit (REST, <http://rest.restfmri.net>) [45] and then obtained the mean ALFF for each PMC subregion by averaging

the ALFF values across all voxels belonging to the subregion.

RSFCs of PMC subregions

We performed whole-brain RSFC analysis on each PMC subregion. Briefly, we first generated a region of interest (ROI) mask for a given PMC subregion and then shrank the mask by removing the voxels in its outer surface. This process partly reduced the biasing effects of the blood oxygenation level dependent (BOLD) signals of the neighboring ROIs. Subsequently, the regional mean time course within the ROI was extracted by averaging the time courses of all the voxels belonging to the ROI. The regional mean time course was further used to compute correlation coefficients with the time courses of all GM voxels. Notably, the computation was constrained within a custom GM mask that was made by thresholding (a probability threshold of 0.2) the GM probability map obtained previously. The resulting correlation coefficients were then converted to z scores using Fisher's r -to- z transform to improve normality. For each subject, we obtained 14 z -score maps indicative of the intrinsic RSFC patterns of the 14 PMC subregions (7 for each hemisphere).

Hierarchical cluster analysis of the RSFC of PMC subregions

To classify PMC subregions with different spatial RSFC patterns, we used a hierarchical cluster analysis. This analysis was conducted only in the HC group to obtain the normal clustering pattern of PMC subregions. Briefly, for each PMC subregion, we first performed a one-sample t -test on the individual RSFC maps to obtain a within-group statistical t map (see statistical analysis section), which was further converted to a standardized Z map to normalize the RSFC strength distribution to a standard normal distribution. The Z maps represent the spatial characteristics of the RSFC patterns of the PMC subregions across the HCs. Subsequently, Pearson's correlation coefficient was computed between pairs of standard Z maps, resulting in a 14×14 correlation matrix. The correlation matrix was then converted to a dissimilarity matrix (i.e., a distance matrix, by subtracting the correlation coefficient from 1), which reflects the spatial dissimilarity of every pair of RSFC maps with respect to PMC subregion. Finally, we generated agglomerative hierarchical cluster trees based on the dissimilarity matrix with the average linkage agglomerative algorithm.

Statistical analysis

To determine differences in the regional fluctuating amplitudes among the PMC subregions and between the AD and HC groups, we applied a repeated measures analysis of covariance (ANCOVA). In this ANCOVA, the subregion was treated as the within-subject factor, and the group was treated as the between-subject factor, with age and gender treated as covariant factors. If a significant effect of group or subregion was found, a subsequent *post hoc* general linear model (GLM) analysis was performed.

To examine the within-group RSFC pattern of each PMC subregion in the AD and HC groups, we performed one-sample *t*-tests in a voxel-wise fashion on the individual RSFC z-score maps of each PMC subregion. The statistical significance level was set at $p < 0.01$ with a cluster size of 18 voxels (486 mm^3) within the custom GM mask, which corresponded to a corrected $p < 0.05$. The cluster size was determined by Monte Carlo simulations [46] using the REST AlphaSim utility (<http://www.restfmri.net>) [45].

To identify between-group differences in the whole-brain RSFC of each PMC subregion, we performed a GLM analysis (dependent variable: RSFCs; independent variable: group), with age and gender treated as covariates. The significance threshold was set at $p < 0.05$ with a cluster size of 43–46 voxels (the number of voxels varied for different PMC subregions), corresponding to a corrected $p < 0.05$. The cluster size for each subregion was determined by Monte Carlo simulations, with the restriction that significant clusters must belong to the significant within-group connectivity map of either of the groups. Given the ambiguous biological interpretations of negative functional connections [47–50], the between-group statistical comparisons were restricted to positive RSFC.

To investigate the relationship between RSFC strength and cognitive behavior, we performed a GLM analysis (dependent variable: RSFC; independent variable: MMSE score) within the regions showing group differences, with age and gender treated as covariates. The statistical significance level was set at $p < 0.05$ with a cluster size of 12–26 voxels (cluster size varied between subregions), corresponding to a corrected $p < 0.05$.

Validation analysis

Effects of grey matter atrophy

Compared to normally aging people, significant GM atrophy in AD patients has been demonstrated in many

previous studies [1, 2]. Therefore, the observed differences in the RSFC of PMC subregions in our study might arise from structural abnormalities in GM volume. To clarify this issue, we re-performed the GLM analysis to test the between-group differences in RSFC of each PMC subregion, with the GM volume map treated as an additional covariate in the GLM [30, 51]. GM volume was calculated using voxel-based morphometry (VBM8 toolbox, <http://dbm.neuro.uni-jena.de/vbm>) [52].

Effects of head motion

Recently, several R-fMRI studies have reported an influence of head motion on functional connectivity [53–55]. To evaluate the effect of head motion on our results, we employed two analysis strategies. First, we re-performed the between-group GLM tests on the RSFC maps of each PMC subregion by regressing out the head motion measures, which were calculated as the root mean square of overall head displacement/rotation [56]. Second, we performed a ‘scrubbing’ procedure on the pre-processed images [55, 57] and then re-calculated the RSFC maps of the PMC subregions and re-performed the within- and between-group statistical tests on the resulting RSFC maps.

RESULTS

Demographics and neuropsychological tests

The demographic characteristics and neuropsychological scores are shown in Table 1. No significant differences in gender or age were observed between the AD and HC groups. However, the MMSE scores in the AD group were significantly lower than those in the control group ($p < 0.0001$).

Automated identification of PMC subdivisions

To detect subregions within the PMC, the module detection method [41] was performed on the PMC backbones extracted from the averaged functional correlation matrices of both the AD patients and HCs. Modularity structure was observed in both of the two groups ($Q = 0.577$ for the AD group and $Q = 0.575$ for the HC group). In the HC group, seven subregions were detected in each hemisphere (Fig. 1G), including the anterior dorsal (ROI 1, red, 420 voxels), posterior dorsal (ROI 2, green, 458 voxels), medial dorsal (ROI 3, blue, 141 voxels), anterior central (ROI 4, cyan, 192 voxels), posterior central (ROI 5, magenta, 294 vox-

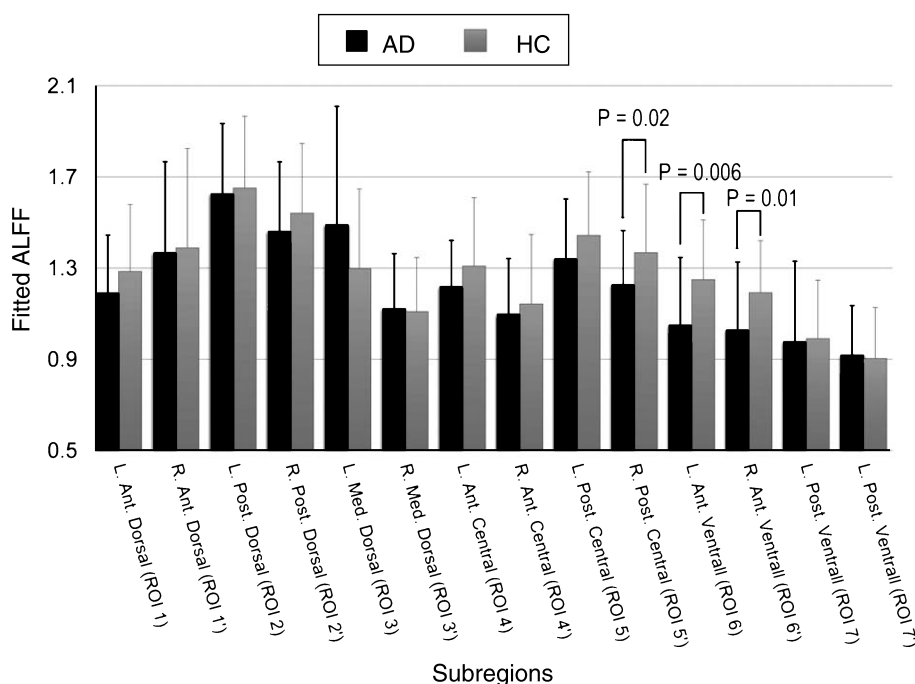


Fig. 2. Repeated measures two-way ANCOVA analysis on the ALFF of PMC subregions. There was no significant subregion effect ($F=0.92$, $p=0.49$) or group effect ($F=2.18$, $p=0.15$), but there was a significant subregion \times group interaction ($F=2.11$, $p=0.047$, Greenhouse-Geisser corrected). Compared to the HC group, the AD group showed significantly reduced ALFF in the left ROI 6 ($p=0.006$), right ROI 6 ($p=0.01$), and right ROI 5 ($p=0.02$). ALFF, amplitude of low-frequency fluctuations; ROI, region of interest; AD, Alzheimer's disease; HC, healthy control.

els), anterior ventral (ROI 6, yellow, 267 voxels), and posterior ventral (ROI 7, brown, 195 voxels) regions. However, in the AD group, only six subregions in each hemisphere were detected (Fig. 1H). The regions comprising the anterior and posterior central modules (i.e., ROIs 4 and 5) in the HC group had been identified as a single medial subregion (cyan region in Fig. 1H) in the AD individuals. Using the module detection method, we further decomposed this medial region into two subregions in each hemisphere ($Q=0.371$, colored cyan and magenta, Fig. 1I), which were highly consistent with those of the HC group based on visual inspection. Between the two groups, the NMI of the PMC subdivision reached 0.86, indicating a high degree of similarity across the modularity partitions.

Regional ALFF changes within PMC subregions

The ANCOVA analysis of PMC subregional ALFF revealed no significant subregion effect ($F=0.92$, $p=0.49$) or group effect ($F=2.18$, $p=0.15$) but a significant group-by-subregion interaction ($F=2.11$, $p=0.047$, Greenhouse-Geisser corrected). *Post-hoc* GLM analysis showed that the ALFF was significantly reduced in the left ROI 6 ($p=0.006$), right ROI 6

($p=0.01$), and right ROI 5 ($p=0.02$) in the AD group compared to the HC group (Fig. 2).

RSFC of PMC subregions

The RSFC maps of each PMC subregion within the HC and AD groups are illustrated in Fig. 3. By visual inspection, the maps showed highly similar patterns between the two groups. Based on the RSFC patterns in the HC group, additional hierarchical clustering analysis classified the seven PMC subregions into three zones along a dorsal-to-ventral gradient (Fig. 4): the anterior dorsal zone (ROI 1); the posterior/medial dorsal zone (ROIs 2–3); and the central/ventral zone (ROIs 4–7). Below, we describe the detailed RSFC patterns of the PMC subregions in terms of their different zones. Given that the RSFC patterns were highly similar between hemispheres, we only reported the results of the left PMC.

Within-group RSFC of PMC subregions

Anterior dorsal zone (ROI 1)

The anterior dorsal zone (ROI 1), located along the marginal ramus of the cingulate sulcus (Fig. 1G, red

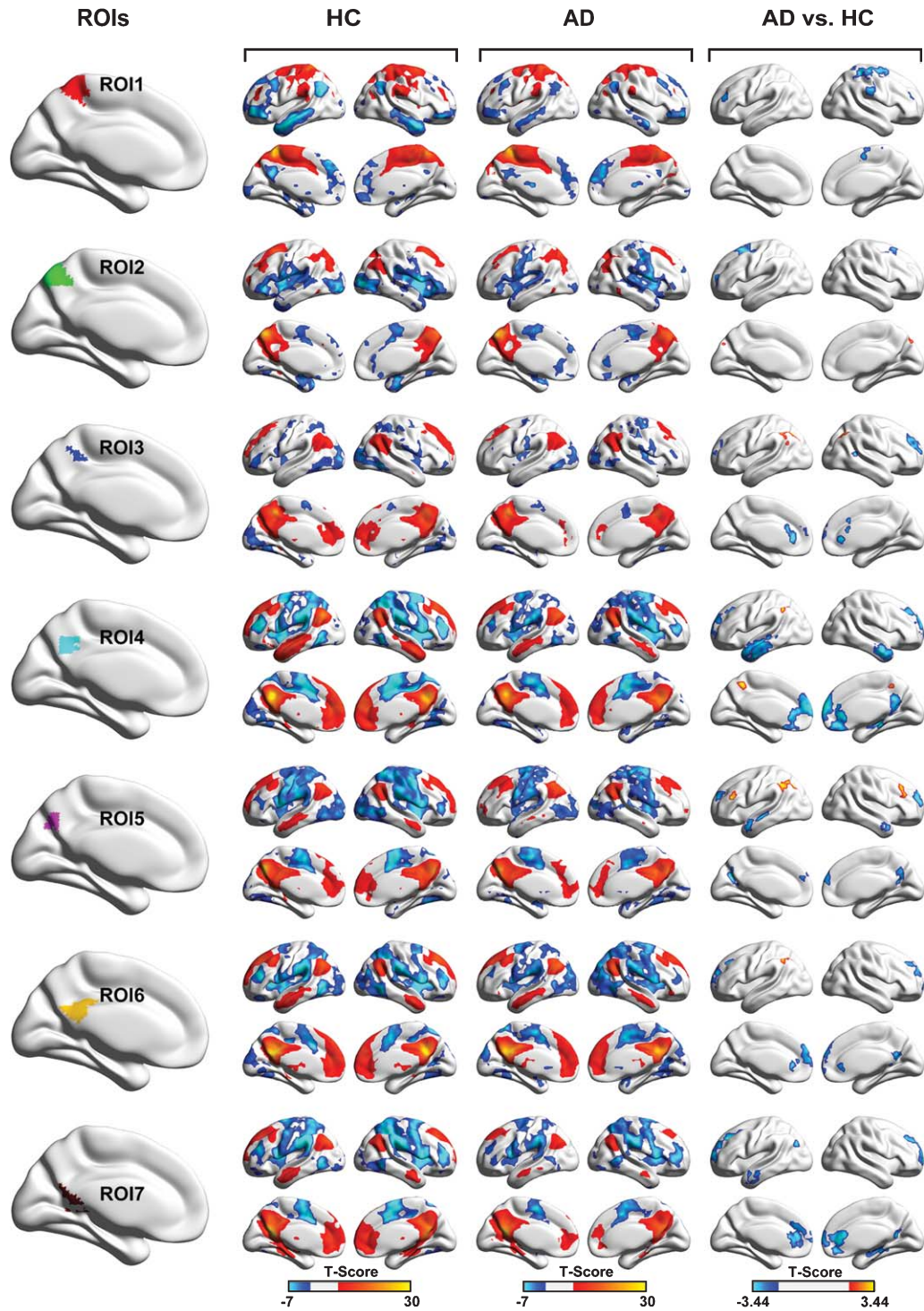


Fig. 3. Resting-state functional connectivity maps of the PMC subregions. The first column shows the PMC subregions detected in the HC group. The second and third columns show the within-group statistical RSFC maps of the HC and AD group, respectively, with a corrected statistical threshold of $p < 0.05$. Hot colors represent positive functional connections, whereas cold colors represent negative functional connections. The last column shows the between-group statistical maps, with a corrected statistical threshold of $p < 0.05$. Hot and cold colors represent increased and decreased functional connectivity, respectively, in the AD group. ROI, region of interest; HC, healthy control; AD, Alzheimer's disease.

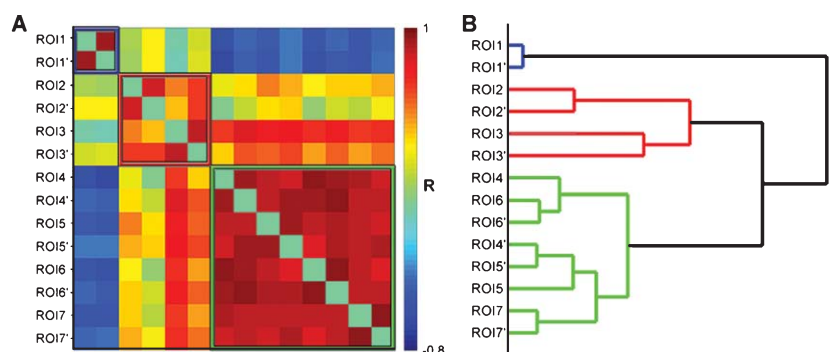


Fig. 4. Spatial hierarchical clustering of PMC subregions in the healthy elderly. A) The correlation matrix was estimated by calculating the Pearson's correlation coefficient between each pair of the within-group subregional RSFC statistical maps. B) Hierarchical clustering based on correlation distance revealed three clusters from the 14 subregions: the anterior dorsal cluster consisting of ROI 1 (blue); the posterior and medial dorsal cluster consisting of ROIs 2–3 (red); and the central and ventral cluster consisting of ROIs 4–7 (green). The apostrophe refers to ROIs within the right hemisphere. ROI, region of interest.

region), exhibited positive RSFC with the precentral gyrus bilaterally, postcentral gyrus bilaterally, supplementary motor area bilaterally, anterior supramarginal gyrus bilaterally, middle frontal gyrus (MFG) bilaterally and superior parietal gyrus (SPG) bilaterally (Fig. 3), which was primarily involved in sensorimotor function. Meanwhile, negative RSFC was observed with typical components of the DMN, including the MPFC, PCC, lateral temporal cortex (LTC), inferior parietal lobe (IPL), and medial temporal lobe (MTL).

Posterior and medial dorsal zone (ROIs 2–3)

The posterior dorsal region (ROI 2), located along the upper part of parieto-occipital fissure (Fig. 1G, green), showed positive functional connectivity with the junction of the precentral and superior frontal sulcus (frontal eye field, FEF) and intraparietal sulcus (IPS) in each hemisphere (Fig. 3), which were identified as the dorsal attention network (DAN). Additionally, connectivity with the IPS extended into parts of the IPL, a component of the DMN. Negative RSFC was found mainly with the visual cortex, temporal pole, insula, supplemental motor area, and MTL. Similar to ROI 2, ROI 3 (the anterior dorsal region located along the cingulate sulcus, Fig. 1G, blue) exhibited significant positive RSFC with the FEF and IPS, components of the DAN, and the IPL and posterior supramarginal gyrus, components of the DMN (Fig. 3). However, ROI 3 exhibited additional positive RSFC with a large cluster that included the MPFC and ventral anterior cingulate cortex (vACC), a core component of the anterior DMN (Fig. 3). Notably, both the posterior and medial dorsal zones (ROIs 2–3) showed no significant connectivity with the LTC, another typical component

of the DMN. These results suggest that the medial dorsal zone (ROI 3) could be a transitive zone between the dorsal and ventral portions of the PMC. Finally, negative RSFC was observed between ROI 3 and the sensorimotor cortex, visual cortex and insula.

Central and ventral zone (ROIs 4–7)

The central and ventral parts of the PMC (ROIs 4–7), which consist of the ventral precuneus and posterior cingulate cortex (Fig. 1G, cyan, magenta, yellow, and brown), shared a highly consistent RSFC pattern. For example, positive RSFC was observed with several DMN regions, including the MPFC/vACC, PCC, LTC and IPL (Fig. 3). Notably, we also observed that the posterior ventral part (ROI 7) exhibited remarkably positive RSFC with the MTL, including the hippocampus and parahippocampus gyrus (Fig. 3). Negative RSFC was found mainly with the sensorimotor cortex, visual cortex, and insula.

Between-group differences in RSFCs of PMC subregions

To avoid the confounding effect of negative RSFC in both statistical analysis and the interpretation of the underlying biological mechanism, we only investigated the positive changes in RSFC in patients with AD. The last column of Fig. 3 illustrates the between-group differences in RSFC for each PMC subregion.

Anterior dorsal zone (ROI 1)

Compared to the HC group, the AD group showed reduced RSFC between the anterior dorsal zone (ROI 1) and the sensorimotor cortex regions, includ-

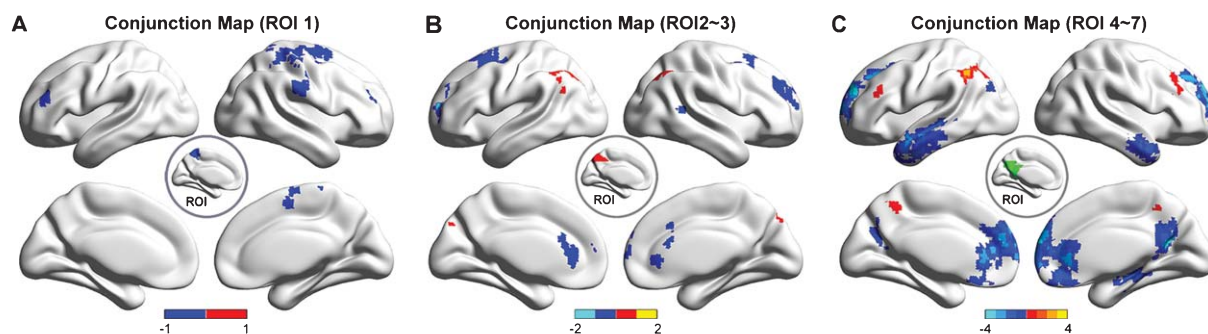


Fig. 5. Conjunction maps of between-group differences in the RSFC of PMC subregions. Between-group differences in RSFC of (A) the anterior dorsal zone (ROI 1); (B) the posterior and medial dorsal zone (ROIs 2–3) and (C) the central and ventral zone (ROIs 4–7). Color bars indicate the frequency with which the region emerged in the between-group comparisons. Hot and cold colors represent increased and decreased functional connectivity, respectively, in the Alzheimer's disease group. ROI, region of interest; RSFC, resting-state functional connectivity.

ing the right precentral gyrus, right postcentral gyrus, right supplementary motor area, right anterior supramarginal gyrus, right SPG, and left MFG (Fig. 3, Fig. 5, and Table 2). There was no significant increase in connectivity with the anterior dorsal zone (ROI 1) in the AD group.

Posterior and medial dorsal zone (ROIs 2–3)

In the AD group, the posterior dorsal zone (ROI 2) showed significantly reduced RSFC with the FEF bilaterally and increased RSFC with the cuneus bilaterally (Fig. 3, Fig. 5, and Table 2). The medial dorsal zone (ROI 3) showed reduced RSFC with the vACC bilaterally, dorsal prefrontal cortex (dPFC) bilaterally and right supramarginal gyrus, and increased RSFC with the IPS bilaterally in the AD group (Fig. 3 and Table 2). A conjunction map in which clusters were included only if they had a significant between-group difference in RSFC with either ROI 2 or 3 is shown in Fig. 5B.

Central and ventral zone (ROIs 4–7)

In the AD group, the central and ventral parts of the PMC (ROIs 4–7) exhibited significantly reduced RSFC with several DMN regions, including the MPFC/vACC, PCC, LTC, IPL, and MTL (Fig. 3 and Table 2). Additionally, we also observed increased RSFC between the central and anterior ventral zone (ROIs 4–6) and the dorsal edge of the left IPL near the IPS, between the posterior central zone (ROI 5) and the dorsal lateral prefrontal cortex (dlPFC) bilaterally and between the anterior central zone (ROI 4) and the medial dorsal precuneus in the AD group (Fig. 3 and Table 2). A conjunction map in which clusters were included only if they had a significant between-group difference in RSFC with any of ROIs 4–7 is shown in Fig. 5C.

Relationship between the RSFC of the PMC subregions and clinical/behavioral variables

In the AD group, we found a significant positive correlation between MMSE score and the functional connections of the PMC subregions, including the RSFC between the right SPG and ROI 1 (blue), the right dPFC and ROI 3 (red), the left inferior temporal gyrus and ROI 4 (green), the left MPFC and ROI 4/ROI 6 (green), the right MPFC and ROI 5/ROI 6 (green), and between the vACC and ROI 7 (green) (Fig. 6). The visualization for RSFC maps were using BrainNet Viewer (<http://www.nitrc.org/projects/bnv/>) [58].

Reproducibility of our results

The effect of GM atrophy

Compared with the controls, the AD patients showed the widespread loss of GM volume over the whole cortex, with the most pronounced loss in the MTL, medial parietal lobe, MPFC/vACC, IPL, insula, and thalamus (Fig. 7A). After regressing out regional GM volume, we found that the between-group differences in RSFC remained significant but with reduced cluster sizes compared to those without GM volume correction (Fig. 7B–D).

The effects of head motion

We evaluated the effect of head motion in two ways: regressing covariance and 'scrubbing'. There were no significant differences in the root mean squares of overall head displacement ($p=0.33$) or in rotation ($p=0.11$) between the two groups. Further statistical analysis in which the root mean squares of overall head displacement/rotation was regressed out revealed very similar results as the previous analysis. After per-

Table 2
Regions showing significant differences of the PMC subregional RSFC in group comparison

ROIs	Brain regions	BA	Cluster voxels	MNI coordinates, mm			Maximum Z score
				x	y	z	
ROI 1	R. PoCG/PrCG/MFG	3/4/6	420	33	-36	60	-3.78
	R. MFG	6	58	6	-3	54	-3.25
	R. PoCG/IPL	3/40	107	51	-21	30	-3.22
	R. CER	NA	52	36	-33	-33	-3.03
	L. MFG	10	67	-33	42	15	-3.02
ROI 2	R. MFG	10	54	33	54	27	-2.88
	L. MFG/SFG	6/8	163	-21	18	60	-3.83
	L. MFG	10	77	-27	45	3	-3.73
	R. MFG	6	126	21	12	45	-3.66
ROI 3	R. CER	NA	53	36	-39	-42	-3.12
	R. PCu	7	49	12	-81	42	2.65
	L. ACG	32	170	0	33	3	-4.74
	R. SFG	9	219	24	48	36	-3.50
	R. STG	22	49	54	-48	9	-3.40
ROI 4	L. SFG/MFG	9/10	108	-12	54	15	-2.87
	L. IPL	40	190	-36	-66	45	4.26
	R. IPL	40	63	36	-72	45	2.93
	R. MTG	21	307	57	-3	-24	-4.27
	R. MFG/SFG	10/9	1436	3	30	-3	-4.27
	R. PHG	36	88	30	-30	-9	-4.03
	L. MTG	21	631	-51	-15	-12	-3.80
ROI 5	R. PCG	31	208	9	-54	27	-3.70
	L. CER	NA	68	-18	-90	-42	-3.40
	L. MFG/SFG	10/9	63	-24	33	45	-3.09
	L. MTG	22	66	-60	-63	24	-2.85
	L. IPL	40	139	-33	-54	39	4.57
	L. PCu	7	73	-9	-51	54	3.77
	R. PCu	7	251	-18	-66	27	-4.31
	L. MTG	21	73	-54	3	-15	-3.93
	R. SFG	10	199	24	54	21	-3.71
	L. SFG	10	124	-18	48	24	-3.59
ROI 6	L. MTG	21	118	-54	-30	-12	-3.42
	R. MTG	21	61	51	9	-27	-3.16
	L. IPL	40	329	-36	-69	39	4.45
	R. MFG	46	156	33	24	36	3.73
	L. MFG	46	58	-36	27	21	3.71
	R. CER	NA	208	15	-84	-18	3.66
	R. CER	NA	68	36	-63	-30	2.77
	R. PCG	31	180	3	-60	15	-3.84
	L. ACG	32	88	-3	30	3	-3.44
	L. MFG/SFG	10/9	70	-24	33	42	-3.12
ROI 7	R. LG	18	100	12	-93	-21	4.06
	L. IPL	40	129	-39	-54	45	3.38
	L. SFG	10	1497	-21	51	21	-4.40
	L. MTG	21	148	-48	-3	-30	-3.38
	R. PCG	23	73	15	-57	12	-3.37
	L. AG	39	55	-45	-78	33	-3.24
R. PHG	36	102	24	-36	-12	-3.16	
L. PCu	7	49	3	-81	33	3.57	

Statistical threshold was set at $p < 0.05$, corrected. ROIs, regions of interest; BA, Brodmann areas; MNI, Montreal Neurological Institute; PoCG, postcentral gyrus; PrCG, precentral gyrus; MFG, middle frontal gyrus; IPL, inferior parietal lobule; CER, cerebellum; SFG, superior frontal gyrus; PCu, precuneus; ACG, anterior cingulate gyrus; STG, superior temporal gyrus; MTG, middle temporal gyrus; PHG, parahippocampal gyrus; PCG, posterior cingulate gyrus; LG, lingual gyrus; AG, angular gyrus; L, left; R, right; NA, not available.

forming the 'scrubbing' procedure on pre-processed images, a mean of 3.13% (range: 0–43.23%, 56 of the 70 individuals were scrubbed less than 5 frames) of volumes were discarded across all subjects. Fur-

ther statistical analysis of the scrubbed data revealed that the majority of the previous results remained largely unchanged. However, for ROIs 4–7, our previous finding of reduced RSFC in the MPFC and

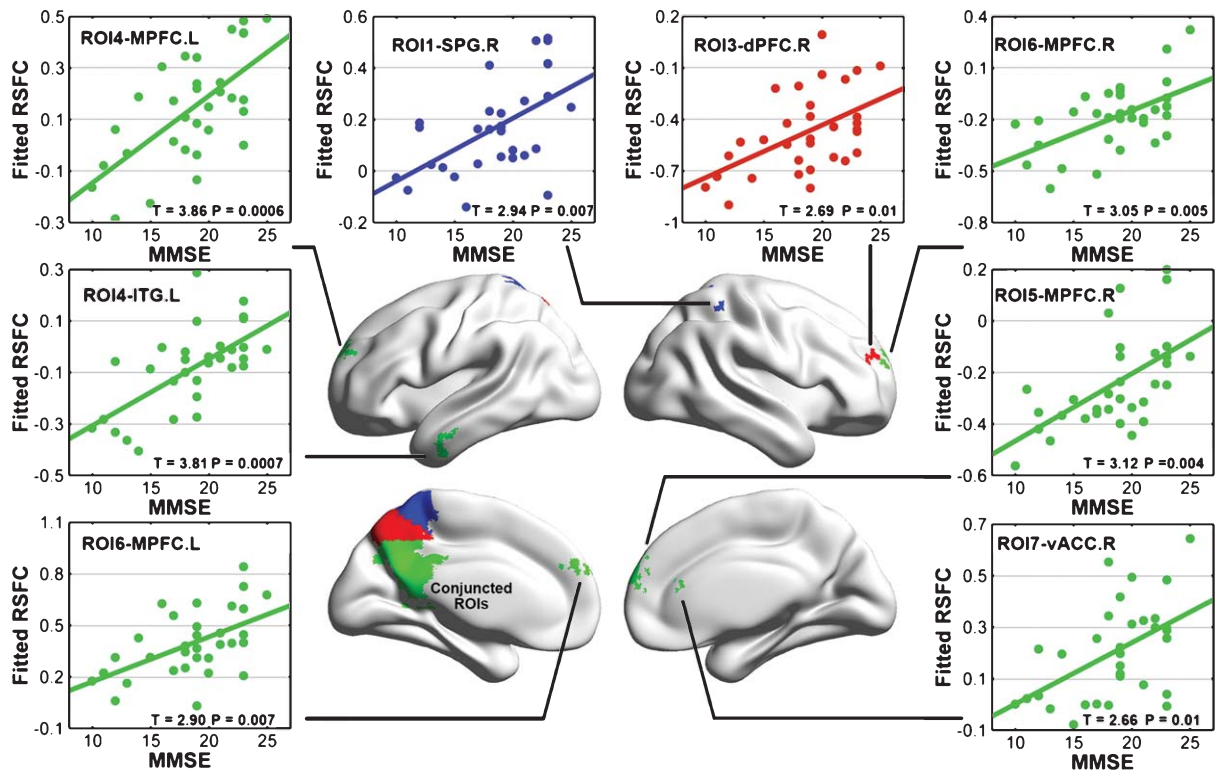


Fig. 6. Correlations between MMSE score and the strength RSFC in PMC subregions. In the AD group, a significant positive correlation ($p < 0.05$, corrected) was found between MMSE score and the functional connectivity of the PMC subregions, including the RSFC between the right SPG and ROI 1 (blue), the right dPFC and ROI 3 (red), the left ITG and ROI 4 (green), the left MPFC and ROI 4/ROI 6 (green), the right MPFC and ROI 5/ROI 6 (green) and the vACC and ROI 7 (green). RSFC, resting-state functional connectivity; MMSE, Mini-Mental State Examination; ROI, region of interest; SPG, superior parietal gyrus; dPFC, dorsal prefrontal cortex; MPFC, middle prefrontal cortex; ITG, inferior temporal gyrus; vACC, ventral anterior cingulate cortex; L, left; R, right.

LTC in the AD group was no longer significant after being corrected for multiple comparisons, although the trend remained after 'scrubbing'. Additionally, we also observed an AD-related reduction in RSFC between the left parahippocampus and ROI 7 (data not shown).

DISCUSSION

Using R-fMRI data and a graph-based module detection algorithm, we subdivided the human PMC in each hemisphere into seven subregions and identified three distinct RSFC patterns. Importantly, we showed that AD patients show differential disruption of the functional connectivity patterns of these PMC subregions and that several of the disruptions in RSFC were correlated with cognitive performance.

Functional connectivity of the PMC subregions

The distributions of the seven PMC subregions were compatible with cytoarchitectonic maps: ROI 1 corre-

sponds to 5 L; ROI 2 to 7A, 7P, and 7M; ROI 3 to 5 M [59]; ROIs 4 and 5 to Brodmann Area (BA) 31; and ROIs 6 and 7 to BA 23 [60]. Furthermore, three distinct RSFC patterns were classified as being functionally connected with the sensorimotor cortex, DAN; and DMN, which are largely consistent with previous R-fMRI studies in young adults [26, 28, 29].

The anterior dorsal zone of the PMC (ROI 1) is functionally connected with the sensorimotor cortex. Tracing studies in monkeys suggest that the caudal and medial portions of the superior parietal lobule (PEc) show anatomical connectivity primarily with the somatomotor-associated cortices [61, 62]. dMRI study in humans has also shown anatomical connections between the PCu and the sensorimotor cortex [19]. Functionally, the anterior dorsal zone of the PMC is involved in motor imagery [13] and spatially guided [63] tasks. Functional connectivity between this zone and the primary motor cortex was also observed using R-fMRI [64, 65]. Thus, our results confirmed these previous findings.

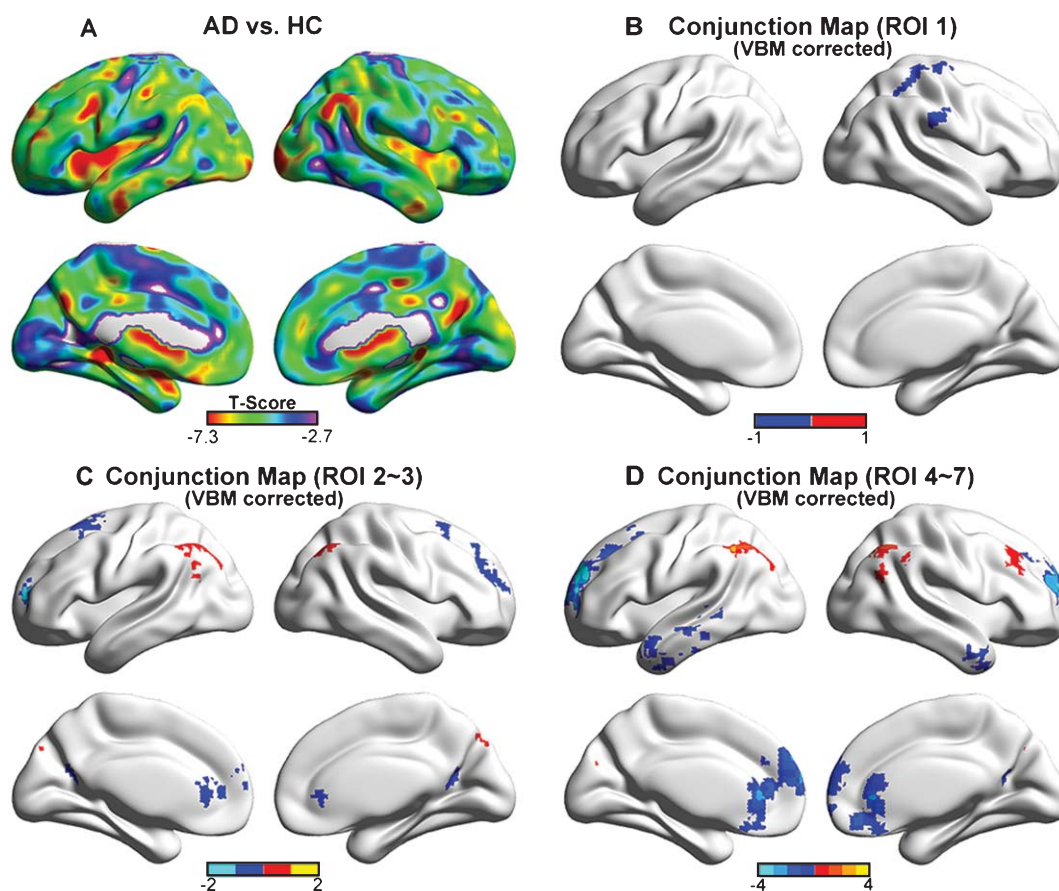


Fig. 7. The effects of GM volume loss on the functional results. A) The between-group differences in GM volume with a threshold of $p < 0.05$, FDR-corrected. The GM volume was corrected during the between-group comparisons of RSFC by adding it as an additional covariate in the GLM analysis. Conjunction maps of the between-group differences in RSFC of (A) the anterior dorsal zone (ROI 1), (B) the posterior and medial dorsal zone (ROIs 2–3) and (C) the central and ventral zone (ROIs 4–7) after GM volume correction.

The posterior and medial dorsal portion of the PMC (ROIs 2 and 3) is primarily functionally connected with the FEF, dPFC and IPS. In monkeys, the medial part of the parietal area (PGm) has anatomical connections with the dPFC [66] and the posterior inferior parietal cortex [23]. In humans, the dPFC and IPS along with the posterior dorsal PCu have been identified as components of the DAN, which is associated with executive processing [67, 68]. Notably, the ROI 3 is additionally connected with the MPFC and IPL, which belong to the DMN. Interestingly, Zhang and colleagues [26] found similar results: the medial zone of PMC (cluster 4 in that study) exhibited RSFC with both the DAN and DMN regions. Collectively, these results suggest the ROI 3 a transitive zone between the dorsal and ventral PCu, and may play a ‘bridge’ role connecting the DAN and DMN.

The central (i.e., ventral PCu) and ventral zones of the PMC (ROIs 4–7) showed significant functional

connectivity with DMN regions. Tract-tracing studies in monkeys have demonstrated that the central and ventral PMC (area 23) are anatomically connected with the MPFC [69], IPL [70] and MTL [71]. Using human dMRI data, Greicius et al. [72] demonstrated that the rostral portion of the PMC is anatomically connected with the MPFC while the caudal portion of the PMC is anatomically connected with the MTL. Moreover, many R-fMRI studies have consistently observed that the PCC exhibits functional connections with the MPFC, LTC, IPL and MTL [17, 73], which are well-known components of the DMN [12]. Recently, Buckner et al. [74] suggested that the ventral PMC, instead of the dorsal PCu, is part of the DMN. This finding was supported by a later PET study in which decreased cerebral blood flow in the PCC, but not dorsal PCu, was observed when subjects performing a spatial working memory task [75]. Our findings are highly consistent with these previous studies. Notably,

the RSFC patterns for this zone are not exactly the same: the ROIs 4 and 6 showed larger spatial extent in the MPFC, while the ROI 7 was more closely connected with the MTL. This finding is largely consistent with anatomical connectivity studies of the human PMC [72].

In the present study, we did not observe significant connections between PMC subregions and visual cortex, which conflicts with the results of previous studies [27–29]. Two potential factors might explain the discrepancy: i) the image pre-processing and parcellation methods were different between previous studies and our work; and ii) the cortical morphology and/or connectivity of the PMC may be affected by aging, since the mean age of the participants in our study is much older than those in previous studies.

Disrupted functional connectivity of PMC subregions in AD

The anterior dorsal zone of the PMC (ROI 1) exhibited reduced functional connectivity with the sensorimotor cortex in AD. Previous structural MRI studies have demonstrated a gradual loss of GM in primary sensorimotor cortex that mirrors the progression of AD severity, suggesting that the structural impairment of the sensorimotor cortex is related to the progression of AD [76]. Furthermore, task-related fMRI studies have reported reduced activation in the SMA and premotor cortex in AD when performing motor-related tasks [77, 78]. Using a transcranial magnetic stimulation paradigm, a recent study showed altered functional connectivity between the posterior parietal cortex and M1 in AD [79]. Combined with these findings, we suggest that, even with clinically subtle motor impairment, the function of the sensorimotor system may be impaired in patients with AD.

The posterior and medial dorsal zones of the PMC (ROIs 2–3) showed reduced functional connectivity with the FEF, dPFC, and MPFC/vACC in AD. The FEF and dPFC are components of the DAN, which is involved in voluntary orienting functions. Our findings are in line with previous R-fMRI studies using independent component analysis, which revealed disrupted functional connectivity of the DAN in AD patients [80] and individuals at high risk for AD [81], suggesting that ‘top-down’ attentional processing mechanisms are impaired in AD. Reduced RSFC was found specifically between ROI 3 and the dPFC and MPFC/vACC, which belong to the DAN and the DMN, respectively. Such a disrupted connectivity pattern might suggest an AD-related decline in the integration of the attention pro-

cessing [67] and the episodic memory processing [7]. Additionally, we noticed increased RSFC between ROI 3 and the IPS bilaterally. Previous studies have found increased fMRI activation in the IPS region in people with AD risk factors when performing a task to distinguish famous names from unfamiliar names, which was considered a compensatory brain response to support task performance [82]. Thus, the increased RSFC of the IPS may suggest a functional hyper-connectivity at baseline underlying task performances in AD.

The central and ventral zones of the PMC (ROIs 4–7) showed reduced RSFC with the DMN regions in AD. The DMN, which is related to episodic memory processing [7], is closely associated with the pathophysiology of AD. PET studies have revealed excess A β accumulation within the DMN regions in AD [21, 83]. Meanwhile, the AD-related GM atrophy is primarily located within these regions [84, 85], and dMRI studies demonstrated reduced fibers connecting the hippocampus and PCC in AD [8]. Functionally, many studies have demonstrated disrupted functional connectivity among various DMN regions in AD [5, 7, 86]. Our findings provide further evidence for the disconnection of the DMN in AD. Additionally, we observed increased RSFC between the left IPL near IPS and ROIs 4–6 and between the bilateral dIPFC and ROI 5. A previous fMRI study using eye movement paradigm demonstrated a left-dominant parietal activation pattern, suggesting a functional lateralization of the left lateral parietal lobe in AD [87]. Recent R-fMRI studies have revealed increased RSFC between the dIPFC and the PCC in AD [86]. Combined with our findings, these increased functional connections might reflect a compensatory recruitment of cognitive resources to maintain task or baseline performance.

Further considerations

Several issues need to be addressed. First, we collected the R-fMRI data from AD patients. Recent studies have paid greater attention to individuals at a high risk for AD, including amnesic mild cognitive impairment [88, 89] and ApoE4 carriers [90, 91]. Investigating these populations would provide predictive insight into the pathophysiology of AD and valuable biomarkers for early clinical diagnosis and intervention. Second, a longitudinal design from MCI-to-AD would be crucial to elucidate dynamic RSFC patterns of PMC subregions. Such an approach might provide predictive insights into understanding the pathophysiological mechanism and disease diagnosis of AD. Third, we employed R-fMRI data

for the connectivity analysis. R-fMRI is a promising technique for measuring spontaneous brain activity; however, it lacks direct observation of anatomical connections. Future studies combining R-fMRI and dMRI data would be helpful to reveal the structural substrates underlying the functional deficits in AD. Finally, we showed that the functional connectivity changes of PMC subregions were correlated with MMSE score in the AD patients. Notably, the MMSE is a comprehensive cognitive evaluation of AD, lacking detailed testing on specific performance. Thus, recruiting more neuropsychological and cognitive tests would be important to assess the PMC subregion-behavior associations.

ACKNOWLEDGMENTS

This work was supported by the Beijing Natural Science Foundation (Grant No. Z111107067311036), Natural Science Foundation of China (Grant Nos. 81000633, 81030028, 31221003, 81370037 and 81000606) and National Science Fund for Distinguished Young Scholars (Grant No. 81225012).

Authors' disclosures available online (<http://www.jalz.com/disclosures/view.php?id=1967>).

REFERENCES

- [1] Busatto GF, Garrido GE, Almeida OP, Castro CC, Camargo CH, Cid CG, Buchpiguel CA, Furuie S, Bottino CM (2003) A voxel-based morphometry study of temporal lobe gray matter reductions in Alzheimer's disease. *Neurobiol Aging* **24**, 221-231.
- [2] Frisoni GB, Testa C, Zorzan A, Sabattoli F, Beltramello A, Soininen H, Laakso MP (2002) Detection of grey matter loss in mild Alzheimer's disease with voxel based morphometry. *J Neurol Neurosurg Psychiatry* **73**, 657-664.
- [3] Delbeuck X, Van der Linden M, Collette F (2003) Alzheimer's disease as a disconnection syndrome? *Neuropsychol Rev* **13**, 79-92.
- [4] He Y, Chen Z, Gong G, Evans A (2009) Neuronal networks in Alzheimer's disease. *Neuroscientist* **15**, 333-350.
- [5] Wang L, Zang Y, He Y, Liang M, Zhang X, Tian L, Wu T, Jiang T, Li K (2006) Changes in hippocampal connectivity in the early stages of Alzheimer's disease: Evidence from resting state fMRI. *Neuroimage* **31**, 496-504.
- [6] Gili T, Cercignani M, Serra L, Perri R, Giove F, Maraviglia B, Caltagirone C, Bozzali M (2011) Regional brain atrophy and functional disconnection across Alzheimer's disease evolution. *J Neurol Neurosurg Psychiatry* **82**, 58-66.
- [7] Greicius MD, Srivastava G, Reiss AL, Menon V (2004) Default-mode network activity distinguishes Alzheimer's disease from healthy aging: Evidence from functional MRI. *Proc Natl Acad Sci U S A* **101**, 4637-4642.
- [8] Zhou Y, Dougherty JH Jr, Hubner KF, Bai B, Cannon RL, Hutson RK (2008) Abnormal connectivity in the posterior cingulate and hippocampus in early Alzheimer's disease and mild cognitive impairment. *Alzheimers Dement* **4**, 265-270.
- [9] Wang K, Liang M, Wang L, Tian L, Zhang X, Li K, Jiang T (2007) Altered functional connectivity in early Alzheimer's disease: A resting-state fMRI study. *Hum Brain Mapp* **28**, 967-978.
- [10] Cavanna AE, Trimble MR (2006) The precuneus: A review of its functional anatomy and behavioural correlates. *Brain* **129**, 564-583.
- [11] Gur RC, Mozley LH, Mozley PD, Resnick SM, Karp JS, Alavi A, Arnold SE, Gur RE (1995) Sex differences in regional cerebral glucose metabolism during a resting state. *Science* **267**, 528-531.
- [12] Raichle ME, MacLeod AM, Snyder AZ, Powers WJ, Gusnard DA, Shulman GL (2001) A default mode of brain function. *Proc Natl Acad Sci U S A* **98**, 676-682.
- [13] Hanakawa T, Immisch I, Toma K, Dimyan MA, Van Gelderen P, Hallett M (2003) Functional properties of brain areas associated with motor execution and imagery. *J Neurophysiol* **89**, 989-1002.
- [14] Addis DR, McIntosh AR, Moscovitch M, Crawley AP, McAndrews MP (2004) Characterizing spatial and temporal features of autobiographical memory retrieval networks: A partial least squares approach. *Neuroimage* **23**, 1460-1471.
- [15] Lundstrom BN, Ingvar M, Petersson KM (2005) The role of precuneus and left inferior frontal cortex during source memory episodic retrieval. *Neuroimage* **27**, 824-834.
- [16] Vogeley K, May M, Ritzl A, Falkai P, Zilles K, Fink GR (2004) Neural correlates of first-person perspective as one constituent of human self-consciousness. *J Cogn Neurosci* **16**, 817-827.
- [17] Fox MD, Snyder AZ, Vincent JL, Corbetta M, Van Essen DC, Raichle ME (2005) The human brain is intrinsically organized into dynamic, anticorrelated functional networks. *Proc Natl Acad Sci U S A* **102**, 9673-9678.
- [18] Hagmann P, Cammoun L, Gigandet X, Meuli R, Honey CJ, Wedeen VJ, Sporns O (2008) Mapping the structural core of human cerebral cortex. *PLoS Biol* **6**, e159.
- [19] Gong G, He Y, Concha L, Lebel C, Gross DW, Evans AC, Beaulieu C (2009) Mapping anatomical connectivity patterns of human cerebral cortex using *in vivo* diffusion tensor imaging tractography. *Cereb Cortex* **19**, 524-536.
- [20] van den Heuvel MP, Sporns O (2011) Rich-club organization of the human connectome. *J Neurosci* **31**, 15775-15786.
- [21] Buckner RL, Sepulcre J, Talukdar T, Krienen FM, Liu H, Hedden T, Andrews-Hanna JR, Sperling RA, Johnson KA (2009) Cortical hubs revealed by intrinsic functional connectivity: Mapping, assessment of stability, and relation to Alzheimer's disease. *J Neurosci* **29**, 1860-1873.
- [22] Liang X, Zou Q, He Y, Yang Y (2013) Coupling of functional connectivity and regional cerebral blood flow reveals a physiological basis for network hubs of the human brain. *Proc Natl Acad Sci U S A* **110**, 1929-1934.
- [23] Pandya DN, Seltzer B (1982) Intrinsic connections and architectonics of posterior parietal cortex in the rhesus monkey. *J Comp Neurol* **204**, 196-210.
- [24] Leichnetz GR (2001) Connections of the medial posterior parietal cortex (area 7m) in the monkey. *Anat Rec* **263**, 215-236.
- [25] Parvizi J, Van Hoesen GW, Buckwalter J, Damasio A (2006) Neural connections of the posteromedial cortex in the macaque. *Proc Natl Acad Sci U S A* **103**, 1563-1568.
- [26] Zhang Y, Fan L, Zhang Y, Wang J, Zhu M, Zhang Y, Yu C, Jiang T (2012) Connectivity-based parcellation of the human posteromedial cortex. *Cereb Cortex*, doi: 10.1093/cercor/bhs353

- [27] Cauda F, Geminiani G, D'Agata F, Sacco K, Duca S, Bagshaw AP, Cavanna AE (2010) Functional connectivity of the posteromedial cortex. *PLoS One* **5**, pii: e13107.
- [28] Margulies DS, Vincent JL, Kelly C, Lohmann G, Uddin LQ, Biswal BB, Villringer A, Castellanos FX, Milham MP, Petrides M (2009) Precuneus shares intrinsic functional architecture in humans and monkeys. *Proc Natl Acad Sci U S A* **106**, 20069-20074.
- [29] Zhang S, Li CS (2012) Functional connectivity mapping of the human precuneus by resting state fMRI. *Neuroimage* **59**, 3548-3562.
- [30] Wang Z, Yan C, Zhao C, Qi Z, Zhou W, Lu J, He Y, Li K (2011) Spatial patterns of intrinsic brain activity in mild cognitive impairment and Alzheimer's disease: A resting-state functional MRI study. *Hum Brain Mapp* **32**, 1720-1740.
- [31] McKhann G, Drachman D, Folstein M, Katzman R, Price D, Stadlan EM (1984) Clinical diagnosis of Alzheimer's disease: Report of the NINCDS-ADRDA Work Group under the auspices of Department of Health and Human Services Task Force on Alzheimer's Disease. *Neurology* **34**, 939-944.
- [32] Ukmar M, Makuc E, Onor ML, Garbin G, Trevisiol M, Cova MA (2008) Evaluation of white matter damage in patients with Alzheimer's disease and in patients with mild cognitive impairment by using diffusion tensor imaging. *Radiol Med* **113**, 915-922.
- [33] Morris JC (1993) The Clinical Dementia Rating (CDR): Current version and scoring rules. *Neurology* **43**, 2412-2414.
- [34] Yan C, Zang Y (2010) DPARSF: A MATLAB Toolbox for "Pipeline" Data Analysis of Resting-State fMRI. *Front Syst Neurosci* **4**, 13.
- [35] Friston KJ, Frith CD, Frackowiak RS, Turner R (1995) Characterizing dynamic brain responses with fMRI: A multivariate approach. *Neuroimage* **2**, 166-172.
- [36] Ashburner J, Friston KJ (2005) Unified segmentation. *Neuroimage* **26**, 839-851.
- [37] He Y, Wang J, Wang L, Chen ZJ, Yan C, Yang H, Tang H, Zhu C, Gong Q, Zang Y, Evans AC (2009) Uncovering intrinsic modular organization of spontaneous brain activity in humans. *PLoS One* **4**, e5226.
- [38] Meunier D, Lambiotte R, Fornito A, Ersche KD, Bullmore ET (2009) Hierarchical modularity in human brain functional networks. *Front Neuroinform* **3**, 37.
- [39] Tzourio-Mazoyer N, Landeau B, Papathanassiou D, Crivello F, Etard O, Delcroix N, Mazoyer B, Joliot M (2002) Automated anatomical labeling of activations in SPM using a macroscopic anatomical parcellation of the MNI MRI single-subject brain. *Neuroimage* **15**, 273-289.
- [40] Foti NJ, Hughes JM, Rockmore DN (2011) Nonparametric sparsification of complex multiscale networks. *PLoS One* **6**, e16431.
- [41] Newman ME (2006) Modularity and community structure in networks. *Proc Natl Acad Sci U S A* **103**, 8577-8582.
- [42] Zang YF, He Y, Zhu CZ, Cao QJ, Sui MQ, Liang M, Tian LX, Jiang TZ, Wang YF (2007) Altered baseline brain activity in children with ADHD revealed by resting-state functional MRI. *Brain Dev* **29**, 83-91.
- [43] Qi R, Zhang LJ, Zhong J, Wu S, Zhang Z, Zhong Y, Ni L, Zheng G, Jiao Q, Wu X, Fan X, Liu Y, Lu G (2012) Dynamic changes of intrinsic brain activity in cirrhotic patients after transjugular intrahepatic portosystemic shunt: A resting-state fMRI study. *PLoS One* **7**, e46681.
- [44] Zuo XN, Di Martino A, Kelly C, Shehzad ZE, Gee DG, Klein DF, Castellanos FX, Biswal BB, Milham MP (2010) The oscillating brain: Complex and reliable. *Neuroimage* **49**, 1432-1445.
- [45] Song XW, Dong ZY, Long XY, Li SF, Zuo XN, Zhu CZ, He Y, Yan CG, Zang YF (2011) REST: A toolkit for resting-state functional magnetic resonance imaging data processing. *PLoS One* **6**, e25031.
- [46] Ledberg A, Akerman S, Roland PE (1998) Estimation of the probabilities of 3D clusters in functional brain images. *Neuroimage* **8**, 113-128.
- [47] Chai XJ, Castanon AN, Ongur D, Whitfield-Gabrieli S (2012) Anticorrelations in resting state networks without global signal regression. *Neuroimage* **59**, 1420-1428.
- [48] Murphy K, Birm RM, Handwerker DA, Jones TB, Bandettini PA (2009) The impact of global signal regression on resting state correlations: Are anti-correlated networks introduced? *Neuroimage* **44**, 893-905.
- [49] Fox MD, Zhang D, Snyder AZ, Raichle ME (2009) The global signal and observed anticorrelated resting state brain networks. *J Neurophysiol* **101**, 3270-3283.
- [50] Weissenbacher A, Kasess C, Gerstl F, Lanzenberger R, Moser E, Windischberger C (2009) Correlations and anticorrelations in resting-state functional connectivity MRI: A quantitative comparison of preprocessing strategies. *Neuroimage* **47**, 1408-1416.
- [51] Bai F, Xie C, Watson DR, Shi Y, Yuan Y, Wang Y, Yue C, Teng Y, Wu D, Zhang Z (2011) Aberrant hippocampal subregion networks associated with the classifications of aMCI subjects: A longitudinal resting-state study. *PLoS One* **6**, e29288.
- [52] Ashburner J, Friston KJ (2000) Voxel-based morphometry—the methods. *Neuroimage* **11**, 805-821.
- [53] Satterthwaite TD, Wolf DH, Loughhead J, Ruparel K, Elliott MA, Hakonarson H, Gur RC, Gur RE (2012) Impact of in-scanner head motion on multiple measures of functional connectivity: Relevance for studies of neurodevelopment in youth. *Neuroimage* **60**, 623-632.
- [54] Van Dijk KR, Sabuncu MR, Buckner RL (2012) The influence of head motion on intrinsic functional connectivity MRI. *Neuroimage* **59**, 431-438.
- [55] Power JD, Barnes KA, Snyder AZ, Schlaggar BL, Petersen SE (2012) Spurious but systematic correlations in functional connectivity MRI networks arise from subject motion. *Neuroimage* **59**, 2142-2154.
- [56] Zuo XN, Kelly C, Di Martino A, Mennes M, Margulies DS, Bangaru S, Grzadzinski R, Evans AC, Zang YF, Castellanos FX, Milham MP (2010) Growing together and growing apart: Regional and sex differences in the lifespan developmental trajectories of functional homotopy. *J Neurosci* **30**, 15034-15043.
- [57] Jenkinson M, Bannister P, Brady M, Smith S (2002) Improved optimization for the robust and accurate linear registration and motion correction of brain images. *Neuroimage* **17**, 825-841.
- [58] Xia M, Wang J, He Y (2013) BrainNet Viewer: A network visualization tool for human brain connectomics. *PLoS One* **8**, e68910.
- [59] Scheperjans F, Hermann K, Eickhoff SB, Amunts K, Schleicher A, Zilles K (2008) Observer-independent cytoarchitectonic mapping of the human superior parietal cortex. *Cereb Cortex* **18**, 846-867.
- [60] Brodmann K (1909) *Vergleichende lokalisationslehre der grobhirnrinde*, Leipzig, Barth.
- [61] Cavada C, Goldman-Rakic PS (1989) Posterior parietal cortex in rhesus monkey: I. Parcellation of areas based on distinctive limbic and sensory corticocortical connections. *J Comp Neurol* **287**, 393-421.
- [62] Cavada C, Goldman-Rakic PS (1989) Posterior parietal cortex in rhesus monkey: II. Evidence for segregated corticocortical

- networks linking sensory and limbic areas with the frontal lobe. *J Comp Neurol* **287**, 422-445.
- [63] Wenderoth N, Debaere F, Snaert S, Swinnen SP (2005) The role of anterior cingulate cortex and precuneus in the coordination of motor behaviour. *Eur J Neurosci* **22**, 235-246.
- [64] Biswal B, Yetkin FZ, Haughton VM, Hyde JS (1995) Functional connectivity in the motor cortex of resting human brain using echo-planar MRI. *Magn Reson Med* **34**, 537-541.
- [65] Fox MD, Snyder AZ, Vincent JL, Raichle ME (2007) Intrinsic fluctuations within cortical systems account for intertrial variability in human behavior. *Neuron* **56**, 171-184.
- [66] Petrides M, Pandya DN (1984) Projections to the frontal cortex from the posterior parietal region in the rhesus monkey. *J Comp Neurol* **228**, 105-116.
- [67] Fox MD, Corbetta M, Snyder AZ, Vincent JL, Raichle ME (2006) Spontaneous neuronal activity distinguishes human dorsal and ventral attention systems. *Proc Natl Acad Sci U S A* **103**, 10046-10051.
- [68] Vincent JL, Kahn I, Snyder AZ, Raichle ME, Buckner RL (2008) Evidence for a frontoparietal control system revealed by intrinsic functional connectivity. *J Neurophysiol* **100**, 3328-3342.
- [69] Morecraft RJ, Cipolloni PB, Stilwell-Morecraft KS, Gedney MT, Pandya DN (2004) Cytoarchitecture and cortical connections of the posterior cingulate and adjacent somatosensory fields in the rhesus monkey. *J Comp Neurol* **469**, 37-69.
- [70] Mesulam MM, Van Hoesen GW, Pandya DN, Geschwind N (1977) Limbic and sensory connections of the inferior parietal lobule (area PG) in the rhesus monkey: A study with a new method for horseradish peroxidase histochemistry. *Brain Res* **136**, 393-414.
- [71] Suzuki WA, Amaral DG (1994) Perirhinal and parahippocampal cortices of the macaque monkey: Cortical afferents. *J Comp Neurol* **350**, 497-533.
- [72] Greicius MD, Supekar K, Menon V, Dougherty RF (2009) Resting-state functional connectivity reflects structural connectivity in the default mode network. *Cereb Cortex* **19**, 72-78.
- [73] Greicius MD, Krasnow B, Reiss AL, Menon V (2003) Functional connectivity in the resting brain: A network analysis of the default mode hypothesis. *Proc Natl Acad Sci U S A* **100**, 253-258.
- [74] Buckner RL, Andrews-Hanna JR, Schacter DL (2008) The brain's default network: Anatomy, function, and relevance to disease. *Ann N Y Acad Sci* **1124**, 1-38.
- [75] Pfefferbaum A, Chanraud S, Pitel AL, Muller-Oehring E, Shankaranarayanan A, Alsop DC, Rohlfing T, Sullivan EV (2011) Cerebral blood flow in posterior cortical nodes of the default mode network decreases with task engagement but remains higher than in most brain regions. *Cereb Cortex* **21**, 233-244.
- [76] Frisoni GB, Prestia A, Rasser PE, Bonetti M, Thompson PM (2009) *In vivo* mapping of incremental cortical atrophy from incipient to overt Alzheimer's disease. *J Neurol* **256**, 916-924.
- [77] Agosta F, Rocca MA, Pagani E, Absinta M, Magnani G, Marccone A, Falautano M, Comi G, Gorno-Tempini ML, Filippi M (2010) Sensorimotor network rewiring in mild cognitive impairment and Alzheimer's disease. *Hum Brain Mapp* **31**, 515-525.
- [78] Vidoni ED, Thomas GP, Honea RA, Loskutova N, Burns JM (2012) Evidence of altered corticomotor system connectivity in early-stage Alzheimer's disease. *J Neurol Phys Ther* **36**, 8-16.
- [79] Bonni S, Lupo F, Lo Gerfo E, Martorana A, Perri R, Caltagirone C, Koch G (2013) Altered parietal-motor connections in Alzheimer's disease patients. *J Alzheimers Dis* **33**, 525-533.
- [80] Li R, Wu X, Fleisher AS, Reiman EM, Chen K, Yao L (2012) Attention-related networks in Alzheimer's disease: A resting functional MRI study. *Hum Brain Mapp* **33**, 1076-1088.
- [81] Sorg C, Riedl V, Muhlau M, Calhoun VD, Eichele T, Laer L, Drzezga A, Forstl H, Kurz A, Zimmer C, Wohlschlagel AM (2007) Selective changes of resting-state networks in individuals at risk for Alzheimer's disease. *Proc Natl Acad Sci U S A* **104**, 18760-18765.
- [82] Seidenberg M, Guidotti L, Nielson KA, Woodard JL, Durgierian S, Antuono P, Zhang Q, Rao SM (2009) Semantic memory activation in individuals at risk for developing Alzheimer disease. *Neurology* **73**, 612-620.
- [83] Buckner RL, Snyder AZ, Shannon BJ, LaRossa G, Sachs R, Fotenos AF, Sheline YI, Klunk WE, Mathis CA, Morris JC, Mintun MA (2005) Molecular, structural, and functional characterization of Alzheimer's disease: Evidence for a relationship between default activity, amyloid, and memory. *J Neurosci* **25**, 7709-7717.
- [84] Scahill RI, Schott JM, Stevens JM, Rossor MN, Fox NC (2002) Mapping the evolution of regional atrophy in Alzheimer's disease: Unbiased analysis of fluid-registered serial MRI. *Proc Natl Acad Sci U S A* **99**, 4703-4707.
- [85] Thompson PM, Hayashi KM, de Zubicaray G, Janke AL, Rose SE, Semple J, Herman D, Hong MS, Dittmer SS, Dordrell DM, Toga AW (2003) Dynamics of gray matter loss in Alzheimer's disease. *J Neurosci* **23**, 994-1005.
- [86] Zhang HY, Wang SJ, Liu B, Ma ZL, Yang M, Zhang ZJ, Teng GJ (2010) Resting brain connectivity: Changes during the progress of Alzheimer disease. *Radiology* **256**, 598-606.
- [87] Thulborn KR, Martin C, Voyvodic JT (2000) Functional MR imaging using a visually guided saccade paradigm for comparing activation patterns in patients with probable Alzheimer's disease and in cognitively able elderly volunteers. *AJNR Am J Neuroradiol* **21**, 524-531.
- [88] Wang J, Zuo X, Dai Z, Xia M, Zhao Z, Zhao X, Jia J, Han Y, He Y (2013) Disrupted functional brain connectome in individuals at risk for Alzheimer's disease. *Biol Psychiatry* **73**, 472-481.
- [89] Bai F, Shu N, Yuan Y, Shi Y, Yu H, Wu D, Wang J, Xia M, He Y, Zhang Z (2012) Topologically convergent and divergent structural connectivity patterns between patients with remitted geriatric depression and amnesic mild cognitive impairment. *J Neurosci* **32**, 4307-4318.
- [90] Brown JA, Terashima KH, Burggren AC, Ercoli LM, Miller KJ, Small GW, Bookheimer SY (2011) Brain network local interconnectivity loss in aging APOE-4 allele carriers. *Proc Natl Acad Sci U S A* **108**, 20760-20765.
- [91] Pievani M, Galluzzi S, Thompson PM, Rasser PE, Bonetti M, Frisoni GB (2011) APOE4 is associated with greater atrophy of the hippocampal formation in Alzheimer's disease. *Neuroimage* **55**, 909-919.